Biophysical Journal, Volume *118*

Supplemental Information

Endothelial Glycocalyx Layer Properties and Its Ability to Limit Leukocyte Adhesion

Luis F. Delgadillo, Graham A. Marsh, and Richard E. Waugh

Supplemental Material

Endothelial Glycocalyx Layer Properties and its Ability to Limit Leukocyte Adhesion.

Luis F. Delgadillo[1], *Graham A. Marsh*[1] *and Richard E Waugh*[1]

[1]*Department of Biomedical Engineering, University of Rochester, Rochester, New York, United States of America*

Derivation of expressions to obtain solutions for the brush model

Our task is to integrate the pressure equation of DeGennes (1) (Eq. 5 of the paper) over the contact region between the EGL and the spherical indenter, then determine the contributions of the EGL indentation and the cell indentation to the total (measured) indentation for a given force. To perform the integration, we note that the value of the radial coordinate r at the edge of the contact zone (R_c) is determined from similar triangles, recognizing that:

$$\frac{L - h_{br}}{R_c} = \frac{R_c}{R_b} \tag{S1}$$

$$\rightarrow R_c = \sqrt{(L - h_{br})R_b} \tag{S2}$$

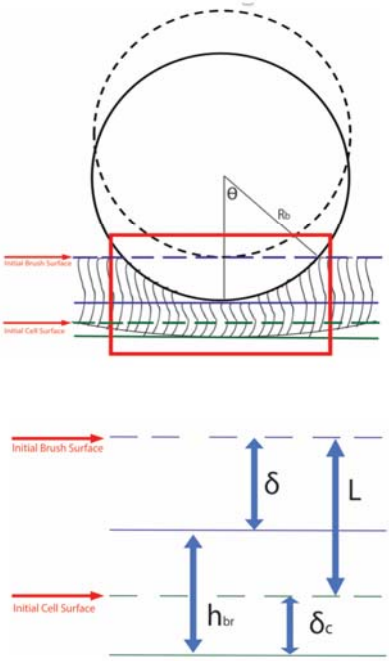

Figure S1. Geometry of interaction of a bead (radius R_b) indenting into a distance δ into the EGL on the surface of a cell. Before the interaction, the height of the brush is L. After indentation, the brush height at the center of the indentation is h_{br}, and the local height $h(r)$ varies with position within the contact region.

where h_{br} is the height of the brush at the center of the contact zone. Integrating the local pressure (Eq. 5) over the contact zone:

$$F_{brush} = \int_{r=0}^{\sqrt{(L-h_{br})R_b}} P(h)dA \tag{S3}$$

where

$$dA = 2\pi r dr \tag{S4}$$

we obtain an expression for the total force as a function of the brush height at the center of the contact region h_{br}. This expression appears in the paper as Equation 6.

$$F_{brush} = \frac{2\pi kT}{s^3}\left[\frac{2}{5}Rh_{br}\left[\left(\frac{h_{br}}{L}\right)^{\frac{5}{4}} - 1\right] - \frac{2}{7}\left[Rh_{br} - h_{br}\left(\frac{L}{h_{br}}\right)^{\frac{3}{4}}\right]\right] \tag{S5}$$

The relationship between the brush height at the center of the indentation and the total indentation measured in the experiment, is complicated by the fact that the surface of the cell is also being displaced (indented) in response to the applied force. The relationships among the indentation variables is illustrated in Figure S1. Before indentation, the brush height is L and the position of the cell surface is defined as zero, After indentation, h_{br} is the

instantaneous brush height at the center of the contact region, δ is the total indentation, and δ_c is the indentation distance into the cell. We note that:

$$\delta_{tot} = \delta_c + L - h_{br} \tag{S6}$$

$$\rightarrow \quad \delta_c = \delta_{tot} + L - h_{br} \tag{S7}$$

To relate the total indentation to the force, we first recognize that the force on the two structures is the same:

$$F_{cell} = F_{brush} \tag{S8}$$

F_{cell} is related to the cell indentation δ_c via the Hertz equation (Eqs. 1 and 2). We can now combine equations 1, 2, S5, S7 and S8 into the form of the equation below

$$0 = \frac{4}{3}\frac{E}{1-\nu^2}\sqrt{r}(\delta_{tot} + L - h_{br}))^{\frac{3}{2}} - 2\pi\frac{kT}{s^3}\left[\frac{2}{5}Rh_{br}\left[\left(\frac{h_{br}}{L}\right)^{\frac{5}{4}} - 1\right] - \frac{2}{7}\left[Rh_{br} - h_{br}\left(\frac{L}{h_{br}}\right)^{\frac{3}{4}}\right]\right] \tag{S9}$$

To obtain h_{br} we will find the roots of the equation (S9) at each indentation point along the force curve. This result appears in the manuscript as Eq. 7.

Rectification of repeated indentation curves

The raw data from each indentation was filtered in Matlab using a Butterworth filter in the Signal Processing Toolbox (The Mathworks, Inc., Natick, MA) to remove 60 Hz noise that was observed in some of the indentations. To align the indentation curves and compensate for any sample drift during the experiment, the data were first fit with a simple Hertz indentation into an elastic half- space, with parameters to account for any non-zero slope of the no-force region and the offset of the contact point:

$$F = \begin{cases} k\delta + b & \delta < C \\ \dfrac{4}{3}\dfrac{E}{1-\nu^2}R^{1/2}\left(\delta - C\right)^{3/2} + k\delta + b & \delta \geq C \end{cases} \tag{S10}$$

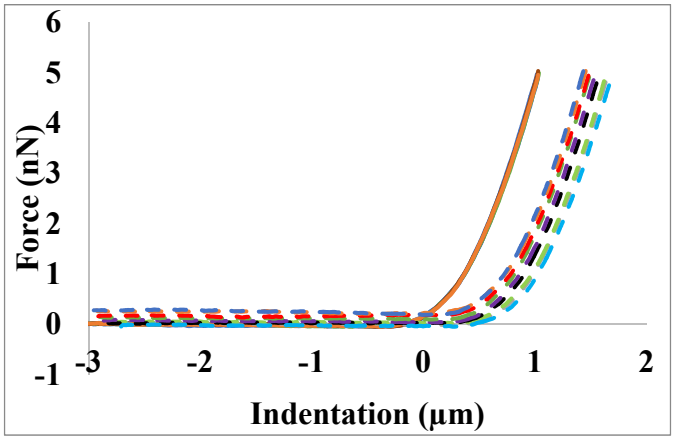

Figure S2. Output curves from the AFM must be registered to compensate for thermal drift during the course of multiple measurements. Typically, 10 curves were obtained at a given location on a cell. Each of the ten curves was fit to Hertz theory for indentation of a simple elastic half space, including factors for displacement and tilt of the data curve. The figure shows ten raw indentation curves before (dashed lines) and after (solid lines) the correction procedure.

The slope and force offset were generally very well corrected with the simplified Hertz theory fit, and we were able to assume that the force away from the cell surface was always zero. When individual, un-averaged, curves were analyzed there was not a significant difference in the measured EGL thickness or modulus between the first and last curve taken on a cell, indicating that we did not damage or alter the cell during the repeated indentation process. The ten curves were then averaged to remove cantilever noise (Figure S2).

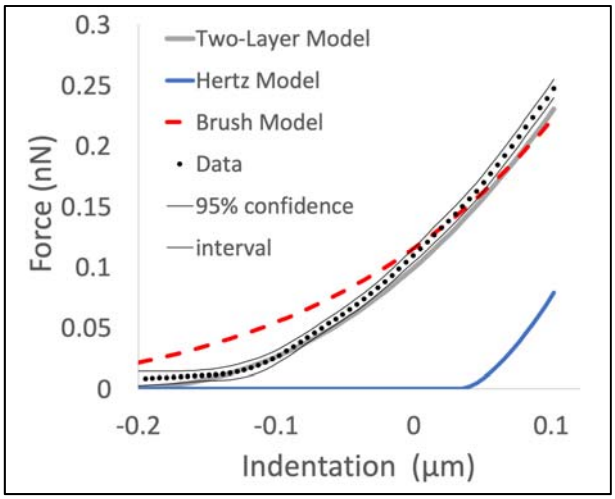

Figure S3. Close-up of the transition region for the data and fits shown in Figure. 1 of the manuscript showing data points calculated from the average of nine indentations and the 95% confidence range for those values.

The fact that we are averaging multiple indentations enables us to estimate confidence intervals for the averaged values at each indentation point after filtering and registering the multiple curves. It is worth noting that the 95% confidence intervals for the mean measured value at each point is small compared to differences in the theoretical predictions. This is shown in Figure S3 for the data of Fig. 1 in the manuscript and additional examples are shown in Figure S5.

Effect of Poisson ratio on predicted indentation curves

Changing the Poisson ratio from 0.1 to 0.5 had a minimal effect on the shape and goodness of fit of the predicted force-indentation curves. This is shown in Figure S4, where three different Poisson ratios were used to fit the same data set.

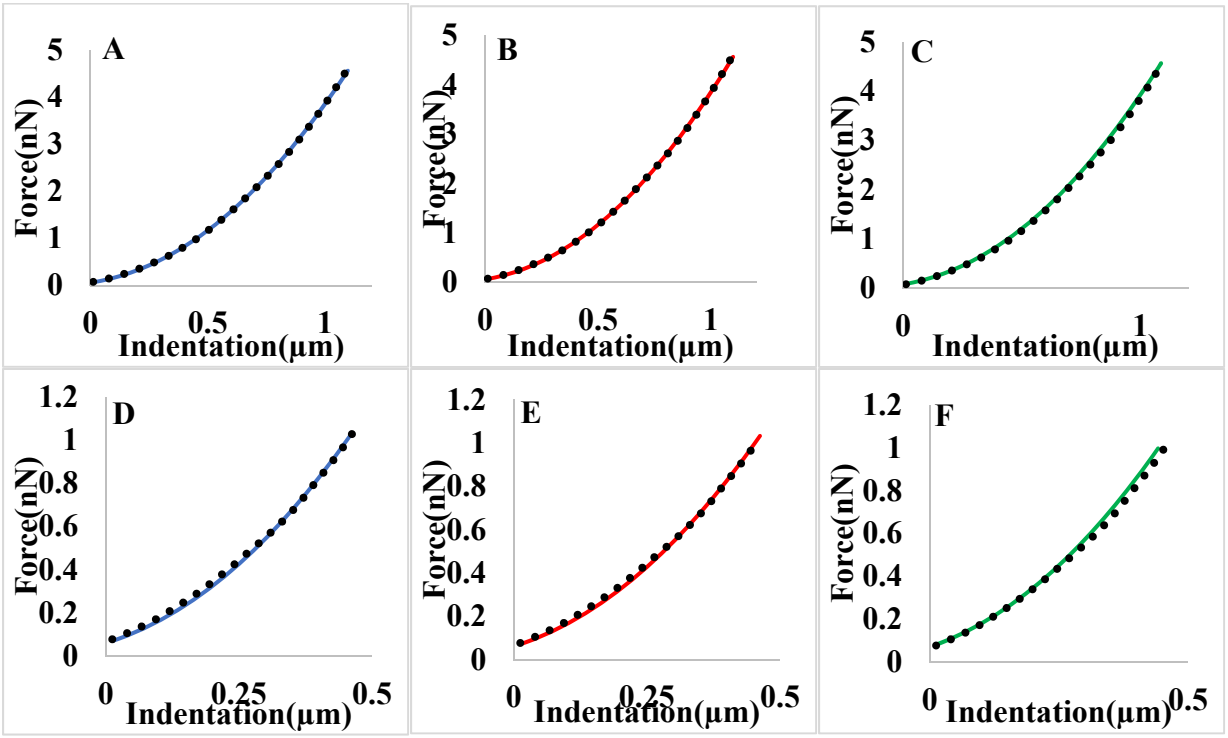

Figure S4. Representative indentation curves with elastic layer model fits using different Poisson ratios. **A** is using Poisson ratio of 0.5 for both the cell body and the glycocalyx. **B** is using values of 0.3 for both the cell body and the glycocalyx. **C** is using 0.1 for both the cell body and the glycocalyx. The second row shows the initial indentation depth (<0.5μm) for each of the Poisson ratios shown in the first row. Visually, the best fits were produced when a Poisson ratio of 0.3 was used for both the cell body and the glycocalyx.

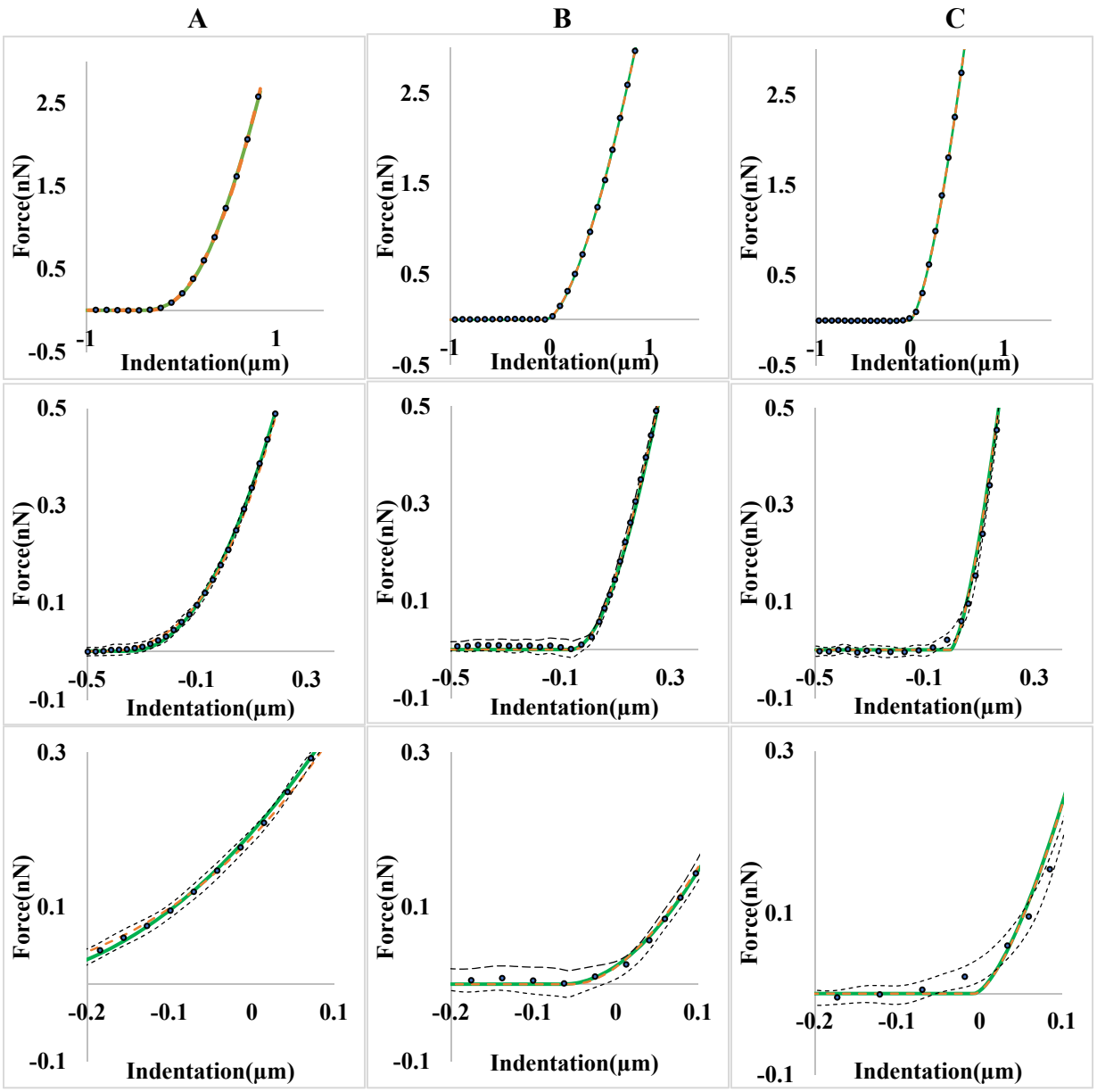

Figure S5. Representative indentation curves with models fits showing the different cases for goodness of fits. Orange curves are the elastic layer model, green curves are the brush model and blue dots are the raw indentation data. Top row: fits for the full range of indentation; second row: the initial contact region; third row: close up of the contact point showing the bands of uncertainty for the means of the measurements. **A** Indentation fit and models where the coefficients of variation for the three fitted parameters were less than 10%. **B** Indentation data and fit where the coefficients of variation were less than 10% for the elastic layer model but not for the brush model. **C** Indentation data where both the elastic layer model and the brush model had coefficients of variation larger than 10% for the three fitted parameters. Curves for the 95% confidence interval of the raw data are given as black dashed lines in the bottom row. Errors in the fits are attributed to noise in the data, usually before contacting the surface.

Modeling details for assessing molecular accessibility

A model of the leukocyte surface, including an array of microvilli with different heights and non-uniform distributions of adhesion molecules was developed in previous publications (6, 7). The size distribution and stiffness of microvilli on the surface of the cell were determined by matching model predictions to measurements of fluorescence intensity using total internal reflectance fluorescence (TIRF) microscopy. For the purposes of modeling the indentation of the cell surface into the EGL, we treat the individual microvilli as springs with spherical caps that are pressed into the EGL. (See Figure 2 in the manuscript.) The distribution of different microvilli heights is illustrated in Figure S6. As described previously, we approximate the distribution of microvillus heights with discrete values, where each of the different values occurs with different frequency as given by the probability distribution. In the present analysis, we used seventeen different discrete heights, with probabilities roughly approximating a log normal distribution.

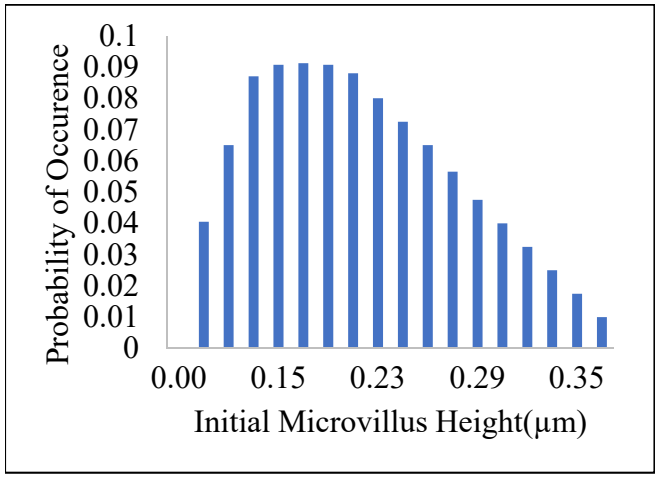

Figure S6. Distribution of microvillus heights used in the indentation analysis. The values follow a lognormal distribution. Discrete values were chosen to reduce computational burden.

A previous analysis of the cell impinging on a smooth rigid surface has shown that as the cell is pressed against the substrate, there is an initial phase where the primary effect is to compress the microvilli (6). A point is reached, however, where the stiffness of the leukocyte is not sufficient to compress the microvilli further, at which point, a flat interface between the cell and the substrate begins to grow at a constant separation distance between the cell and the surface (Figure S7) (6). It is at this point that the indentation of the microvilli into the EGL would be maximized. Recognizing that the resistance of the endothelial cell to indentation is much greater than the resistance of the neutrophil microvilli to

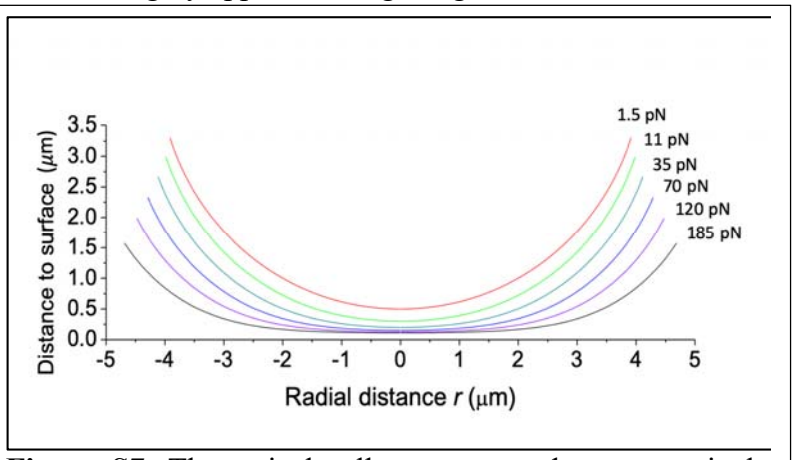

Figure S7. Theoretical cell contours under progressively increasing impingement force onto a flat substrate. (Re-plotted from (3).) A stiff substrate is located on the *x*-axis, and the space between the axis and an individual curve is occupied by the microvilli. At low forces the distance between the center of the contour and the substrate decreases as the microvilli are compressed. When the force reaches about 70 pN, the microvilli are maximally compressed (because the cell is not stiff enough to compress them further) and a region of close contact increases in size as the force continues to increase.

compression, we treat the cell as a rigid substrate and model the interaction between microvilli indenting an EGL layer of defined thickness and modulus layered over a rigid endothelium.

Geometry of Interaction. A schematic of the leukocyte surface pressing into the EGL is shown in Figure 2 of the manuscript. The EGL has thickness t and modulus E_{GC}. The distance the leukocyte is displaced toward the endothelium is z and the point at which the longest microvillus first touches the EGL is taken to be $z = 0$. At $z = 0$, the distance between the i^{th} microvillus and the EGL is z_{0i}. When $z < z_{0i}$, the i^{th} microvillus has yet to contact the EGL. When $z > z_{0i}$, the microvillus indents the EGL and both the microvillus and the EGL are compressed. Thus, when a microvillus begins to penetrate into the EGL layer, there is a deflection of the EGL layer due to the microvillus penetration δ_{Gi} and a deflection of the microvillus δ_{Mi}, and these are related to displacement distance z by:

$$\delta_{Gi} + \delta_{Mi} = z - z_{0i}\,, \qquad z > z_{0i}\,, \delta_{Gi} < t \tag{S11}$$

The microvillus is stiffer than the EGL, and therefore the longest microvilli may eventually penetrate the entire thickness of the EGL and contact the endothelium. Under these conditions, $\delta_{Gi} = t$, and δ_{Mi} is given by:

$$\delta_{Mi} = z - z_{0i} - t, \qquad \delta_{Gi} = t \tag{S12}$$

Thus, there are essentially three types of interaction for each microvillus in the region of contact (Figure 2B of the manuscript). In region I, the microvillus has not yet contacted the EGL and retains its resting dimensions. In region II the microvillus is penetrating the EGL, but has not reached the endothelial surface, and in region III, the EGL is fully penetrated and the microvillus contacts the endothelial surface. Calculations for region I are trivial: there is no force exerted by the microvillus and there are no molecules within range of bonding with the surface. In region III, calculations are straightforward, as the microvillus deflection can be calculated directly from the displacement z. In region II, the relative deflections of the microvillus and the EGL must be determined by equating the microvillus compression force with the EGL indentation force.

Force Relations. We treat the microvilli as simple springs with a common spring constant k_M. In this case the microvillus force F_{Mi} is simply proportional to the deflection δ_{Mi}:

$$F_{Mi} = k_M \delta_{Mi} \tag{S13}$$

To calculate the reaction force of the EGL, we use the expression developed by Dimitriadis (8) for a thin film on an incompressible substrate. We assume the Poisson ratio of the EGL is 0.5 such that the expression for the EGL force corresponding to the i^{th} microvillus F_{Gi} is:

$$F_{Gi} = \begin{cases} 0 & z < z_{0i} \\ \dfrac{16}{9} E_{GL} R_M^{1/2} \delta_{Gi}^{3/2} \left[1 + 1.133\,\chi_{Gi} + 1.283\,\chi_{Gi}^2 + \ldots \right. & 0 \le \delta_{Gi} \le t \\ \qquad \left. \ldots + 0.769\,\chi_{Gi}^3 + 0.0975\,\chi_{Gi}^4 \right] & \end{cases} \tag{S14}$$

where $\chi_{Gi} = \sqrt{R_M \delta_{Gi}}\,/t$. To determine the deflections of the microvillus and the EGL and the corresponding force for region II, we solve Eqs. S11, S13 and S14 numerically for the condition $F_G = F_M$.

To proceed numerically, we increase z stepwise, and for each value of z we assess the force contribution from each of the microvillus initial heights, and perform a weighted sum of each contribution:

$$F_{tot} = \sum_{i=1}^{n} p_i F_{Mi} \tag{S15}$$

where n is the number of different microvillus heights, and p_i is the probability that a given microvillus will have the initial height h_{Mi}. The quantity F_{tot}, when multiplied by the density of microvilli on the surface, gives the contact stress in the interface. When the contact stress reaches the maximum stress that the cell can exert, calculations are halted and the final values for z, and δ_{Mi} are tabulated for calculating the accessibility of molecules to the endothelial surface. The maximum stress that the cell can exert is the pressure inside the cell, and this is estimated by treating the neutrophil as a fluid droplet (9) and using published values of the cell cortical tension (20 pN/μm (4, 5)) and Laplace's law:

$$\sigma_{\max} = P_c = \frac{2\bar{T}_{cort}}{R_c} \tag{S16}$$

The parameter values used in the calculations are given in Table S1. The spring constant of the leukocyte microvillus was taken from work by Hocde (2). The maximum height of the microvilli, the radius of the cell, and the approximate radius of the tip of the microvilli are based on scanning electron micrographs, light microscopy, and observations of fluorescently labeled neutrophils using TIRF microscopy (7).

	High Shear (10 Dynes/cm$^{2)}$	**Low Shear (0.5 Dynes/cm^2)**	**units**
t	0.11	0.065	μm
E_{GL}	25	25	Pa
h_{max}	0.37	0.37	μm
k_M	38	38	pN/μm
R_M	100	100	nm
R_C	4	4	μm
Bond %	1.7%	2.4%	

Table S1. Parameters used in the calculation of the force vs. distance curves for the two simulation cases. The thickness of the EGL, t and the modulus of the EGL, E_{GL}, were the values calculated using the elastic-layer model. The spring constant of the microvillus, k_M, is adopted from work by Hocde (2). The maximum height of the microvillus, h_{max}, was obtained from Lomakina et al. (3). The radius of the microvillus, R_M, and the radius of the cell, R_C, were approximated from observations of leukocytes. The percentages of molecules within range of bonding (40 nm) were calculated as described in the text. The cell cortical tension was taken to be 20 pN/μm(4, 5).

In some situations, the microvilli might all be completely embedded in the EGL, and the body of the cell may contact the EGL. At this point, the leukocyte surface is typically flat, or has a very small curvature, making the forces required to indent the EGL very large. In this case, we assume that further penetration of the EGL does not occur. Numerically, we monitor the separation distance between the cell body and the EGL ($h_{max} - z$) and if this quantity becomes negative, indentation is halted.

Fraction of molecules available for bonding.

To determine what fraction of molecules on the surface are available for bonding, we apply our previous observations of the distribution of molecules relative to cell surface topography (2, 7). Our prior studies indicate that β_2 integrins and chemokine receptors tend to be sequestered away from the tips of microvilli and concentrate in the valleys between the microvilli. In this case, the probability of finding a molecule a certain distance from the tip of the microvillus is well

described by a *beta* distribution. In the present context we focus on the distribution of LFA-1 because of its important role in cell arrest and firm attachment to the endothelium during the inflammatory response. The beta distribution takes the form:

$$\beta(Q;c,d)=\begin{cases}\dfrac{\Gamma(c+d)}{\Gamma(c)\Gamma(d)}Q^{c-1}(1-Q)^{d-1} & \text{if } Q\in[0,1]\\ 0 & \text{otherwise}\end{cases} \tag{S17}$$

where Q is the ratio of the distance of a molecule from the cell body to the instantaneous height of the microvillus, and Γ is the gamma function. The probability density function gives the likelihood that the molecule will be found at the position denoted by Q. Based on TIRF measurements of labeled LFA-1, the distribution of LFA-1 is well-described for values of the parameters c and d of 2.5 and 1.0 respectively (2, 7). Using these values and the calculated values for the compressed microvillus height and the distance of the microvillus tip from the endothelium, we can estimate the percentage of molecules within a certain distance of the endothelium.

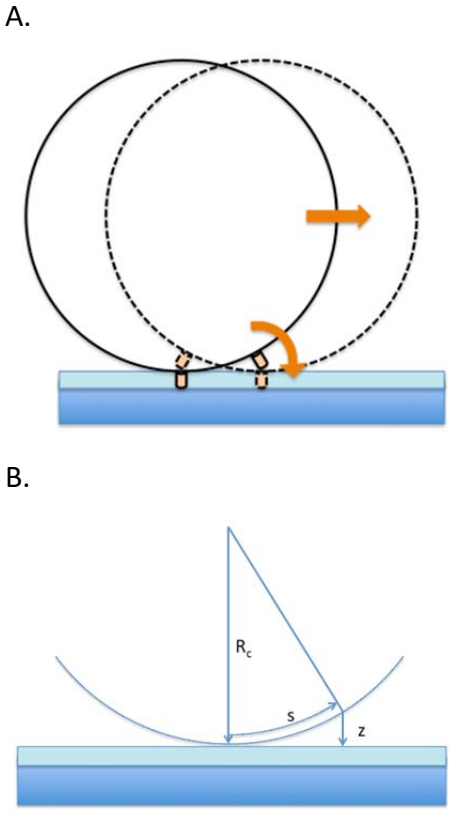

Figure S8. A. Schematic of a rolling neutrophil showing the displacement of a microvillus projection on the cell surface into the EGL as the cell rolls forward. **B.** Schematic of the coordinate values used in the calculations. The cell radius is R_c, the distance along the spherical cell surface is s, and the distance from a point on the leukocyte surface to the EGL is z.

Velocity of indentation of a microvillus on a rolling neutrophil

An important question to address is whether the rates of indentation used in AFM experiments are physiologically appropriate. To estimate indentation rates that might occur in vivo, we consider a neutrophil rolling on an endothelial surface at a velocity v_r. We model the cell as a sphere with radius R_c, and address the question, how rapidly do points on the sphere approach the surface as the cell rolls forward (Fig. S8). At time zero we let s be the surface position measured along the spherical contour from the point of contact. The vertical distance z from the surface at position s is

$$z = s\sin\left(\frac{s}{R_c}\right) \tag{S18}$$

The position s is related to the velocity of rolling and time, t:

$$s = v_r t \tag{S19}$$

The instantaneous velocity of indentation at a point s on the surface is simply the time derivative of z:

$$\frac{dz}{dt} = v_r \sin\left(\frac{v_r t}{R_c}\right) + \frac{v_r^2 t}{R_c}\cos\left(\frac{v_r t}{R_c}\right) \tag{S20}$$

Applying the small angle approximation, we find:

$$\frac{dz}{dt} \approx \frac{2 s v_r}{R_c} \tag{S21}$$

Using Eq. S21, and known values for the relevant parameters, we can estimate the indentation velocity. Kim and Sarelius measured rolling velocities in post capillary venules in the mouse (when fully engaged with endothelium) of 27 μm/s (10). In previous work in which we evaluated the change in fluorescence intensity in TIRFM as neutrophils spread onto a glass surface, we found a maximum microvillus height of approximately 370 nm, and a most probable height of approximately 175 nm (7). Taking the cell radius to be 4.0 μm, we can calculate the instantaneous velocity component of the neutrophil surface toward the endothelium (Figure S9). The indentation velocity depends on the position of the microvillus relative to the center of the contact site. For an initial separation distance of 370 nm, the velocity ranges from approximately 16 μm/s to zero, with an average velocity of approximately 8 μm/s. For a more typical microvillus height (180 nm) the indentation velocity ranges from approximately 11 μm/s to zero, with an average velocity of 5.7 μm/s. These values are consistent with indentation rates used in most AFM studies of EGL properties, and are within the range where the EGL exhibits elastic behavior.

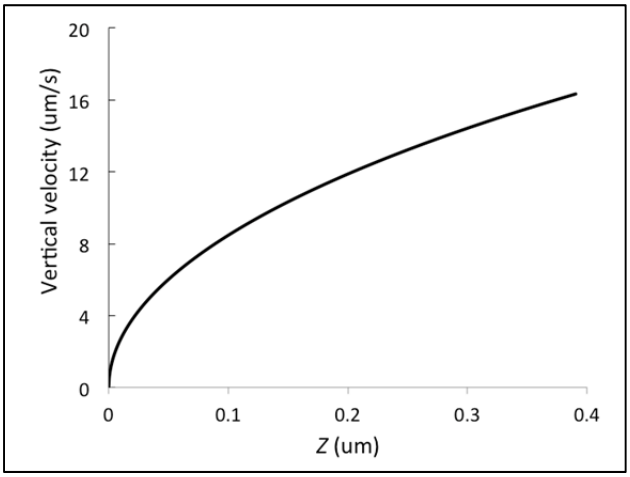

Figure S9. Vertical velocity of a point on the surface of a cell rolling at a velocity of 27 μm/s as a function of its distance from the surface.

Bibliography

1. de Gennes, P. G. 1987. Polymers at an interface; a simplified view. Advances in Colloid and Interface Science 27:189-209.
2. Hocde, S. A., O. Hyrien, and R. E. Waugh. 2009. Cell adhesion molecule distribution relative to neutrophil surface topography assessed by TIRFM. Biophys J 97(1):379-387.
3. Lomakina, E. B., G. Marsh, and R. E. Waugh. 2014. Cell surface topography is a regulator of molecular interactions during chemokine-induced neutrophil spreading. Biophys J 107(6):1302-1312.
4. Lomakina, E. B., C. M. Spillmann, M. R. King, and R. E. Waugh. 2004. Rheological analysis and measurement of neutrophil indentation. Biophys J 87(6):4246-4258.
5. Needham, D., and R. M. Hochmuth. 1992. A sensitive measure of surface stress in the resting neutrophil. Biophys J 61(6):1664-1670.

6. Hocde, S. A., O. Hyrien, and R. E. Waugh. 2009. Molecular accessibility in relation to cell surface topography and compression against a flat substrate. Biophys J 97(1):369-378.
7. Lomakina, E. B., G. Marsh, and R. E. Waugh. 2014. Cell Surface Topography Is a Regulator of Molecular Interactions during Chemokine-Induced Neutrophil Spreading. Biophysical Journal 107(6):1302-1312.
8. Dimitriadis, E. K., F. Horkay, J. Maresca, B. Kachar, and R. S. Chadwick. 2002. Determination of elastic moduli of thin layers of soft material using the atomic force microscope. Biophysical Journal 82(5):2798-2810.
9. Evans, E., and B. Kukan. 1984. Passive material behavior of granulocytes based on large deformation and recovery after deformation tests. Blood 64(5):1028-1035.
10. Kim, M. B., and I. H. Sarelius. 2004. Role of shear forces and adhesion molecule distribution on P-selectin-mediated leukocyte rolling in postcapillary venules. Am J Physiol Heart Circ Physiol 287(6):H2705-2711.